



# Fluid Discrimination in Ultra-Deep Reservoirs Based on a Double Double-Porosity Theory

Xinyang Zhou<sup>1</sup>, Jing Ba<sup>1\*</sup>, Juan E. Santos<sup>2,3</sup>, José M. Carcione<sup>1,4</sup>, Li-Yun Fu<sup>5</sup> and Mengqiang Pang<sup>1</sup>

<sup>1</sup> School of Earth Sciences and Engineering, Hohai University, Nanjing, China, <sup>2</sup> Laboratorio de Geofísica Numérica, Instituto del Gas y del Petróleo, Facultad de Ingeniería, Universidad de Buenos Aires, Buenos Aires, Argentina, <sup>3</sup> Department of Mathematics, Purdue University, West Lafayette, IN, United States, <sup>4</sup> National Institute of Oceanography and Applied Geophysics, Trieste, Italy, <sup>5</sup> Key Laboratory of Deep Oil and Gas, China University of Petroleum, Qingdao, China

## OPEN ACCESS

### Edited by:

Pier Paolo Bruno,  
University of Naples Federico II, Italy

### Reviewed by:

Per Avseth,  
Norwegian University of Science  
and Technology, Norway  
Ken Ikeda,  
The University of Texas at Austin,  
United States

### \*Correspondence:

Jing Ba  
jingba@188.com

### Specialty section:

This article was submitted to  
Solid Earth Geophysics,  
a section of the journal  
Frontiers in Earth Science

**Received:** 06 January 2021

**Accepted:** 06 April 2021

**Published:** 04 May 2021

### Citation:

Zhou X, Ba J, Santos JE,  
Carcione JM, Fu L-Y and Pang M  
(2021) Fluid Discrimination  
in Ultra-Deep Reservoirs Based on  
a Double Double-Porosity Theory.  
*Front. Earth Sci.* 9:649984.  
doi: 10.3389/feart.2021.649984

We develop a methodology, based on rock-physics templates, to effectively identify reservoir fluids in ultra-deep reservoirs, where the poroelasticity model is based on the double double-porosity theory. P-wave attenuation, the ratio of the first Lamé constant to mass density ( $\lambda/\rho$ ) and Poisson ratio are used to build the templates at the ultrasonic and seismic frequency bands to quantitatively predict the total and crack (soft) porosities and oil saturation. Attenuation on these frequency bands is estimated with the spectral-ratio and frequency-shift methods. We apply the methodology to fault-controlled karst reservoirs in the Tarim Basin (China), which contain ultra-deep hydrocarbon resources with a diverse pore-crack system, low porosity/permeability and complex oil-water spatial distributions. The results are consistent with well-log data and actual oil recovery. Crack porosity can be used as an indicator to find regions with high oil saturation, since high values implies a good pore connectivity.

**Keywords:** double double-porosity theory, fault-controlled karst reservoirs, fluid detection, ultra-deep reservoirs, 3D rock-physics template

## INTRODUCTION

With the depletion of relatively shallow conventional reservoirs, ultra-deep resources will become an important target for oil and gas exploration. Carbonate reservoirs are typical examples (e.g., Zou et al., 2014), which, due to their burial depth and high degree of diagenesis, their pay zone is located in areas with secondary pores or cracks (or rift caves and karst caves) (Pang, 2010). The tectonic action, abnormal high pressure, the presence of fractures and thermal fluid activity favor the development of this secondary pore space. Fracture-cavern carbonate reservoirs are among the most important types (Tian et al., 2017; Li et al., 2019). A “fault-controlled karst reservoir” is a large-scale fracture-cavern carbonate reservoir formed by a series of geological processes including the dissolution of atmospheric fresh water or hydrothermal fluid that flows along faults and associated complex fracture system under unexposed conditions (Lan et al., 2015).

The fabric of carbonate rocks has at least two dissimilar porosities, leading to a heterogeneous distribution of immiscible fluids or patchy saturation (Ba et al., 2017). Early models consider a single porosity, such as that of White (1975), who assumed patchy saturation with spherical gas inclusions, and a generalization to non-spherical patches by Johnson (2001). Then,

Pride et al. (2004) studied attenuation caused by patchy saturation based on a double-porosity theory, while Dvorkin and Nur (1993) combined the Biot and squirt flow mechanisms into a set of poroelasticity equations, explicitly considering attenuation due to global flow at cracks or grain contacts. The model has been applied to predict wave velocity and attenuation (Dvorkin et al., 1994, 1995). Deng et al. (2015) extended the squirt-flow model and Tang (2011) analyzed the effect of fractures on the elastic waves. Ba et al. (2011) introduced the Biot-Rayleigh theory to model wave propagation in double-porosity media with a single saturating fluid, and Ba et al. (2017) extended this model to the case of two fluids, i.e., a double double-porosity medium model (DDP).

Rock-physics templates (RPT) relate the reservoir and seismic properties (Odegaard and Avseth, 2004; Carcione and Avseth, 2015). For instance, Chi and Han (2009) interpreted the lithology and obtained fluid content by using RPTs and logging data, and RPTs were used to compute reservoir porosity and oil/gas saturation by Michel (2010). Picotti et al. (2018) analyzed the effects of different fluid saturations, porosities, and permeabilities on seismic waves, and introduced an attenuation RPT for sandstone reservoirs. Pang et al. (2020) estimated the microfracture porosity in carbonate reservoirs by using these attenuation templates. Tran et al. (2020) predicted organic matter content of source rocks using RPTs.

Building a RPT implies to choose the proper properties sensitive to lithology or fluid type and saturation (Batzle et al., 2001; Dillon et al., 2003; Qiao and An, 2007). Goodway et al. (1997) proposed to identify and detect reservoir fluids by using the Lamé constants. Hedlin (2000) proposed the pore modulus as a fluid recognition factor through experiments to distinguish shale, calcite, gas sand, oil sand, and wet sand. The Gassmann fluid term and its product with mass density were used as a fluid discriminator by Russell et al. (2003, 2006), and Quakenbush et al. (2006) used Poisson's ratio for the same purpose. Quintal (2012) suggested that frequency-dependent attenuation due to wave-induced fluid flow is a potential index of saturation, and Xue et al. (2017) used a combination of the normal crack compliance of the saturated and dry rocks as a fluid factor.

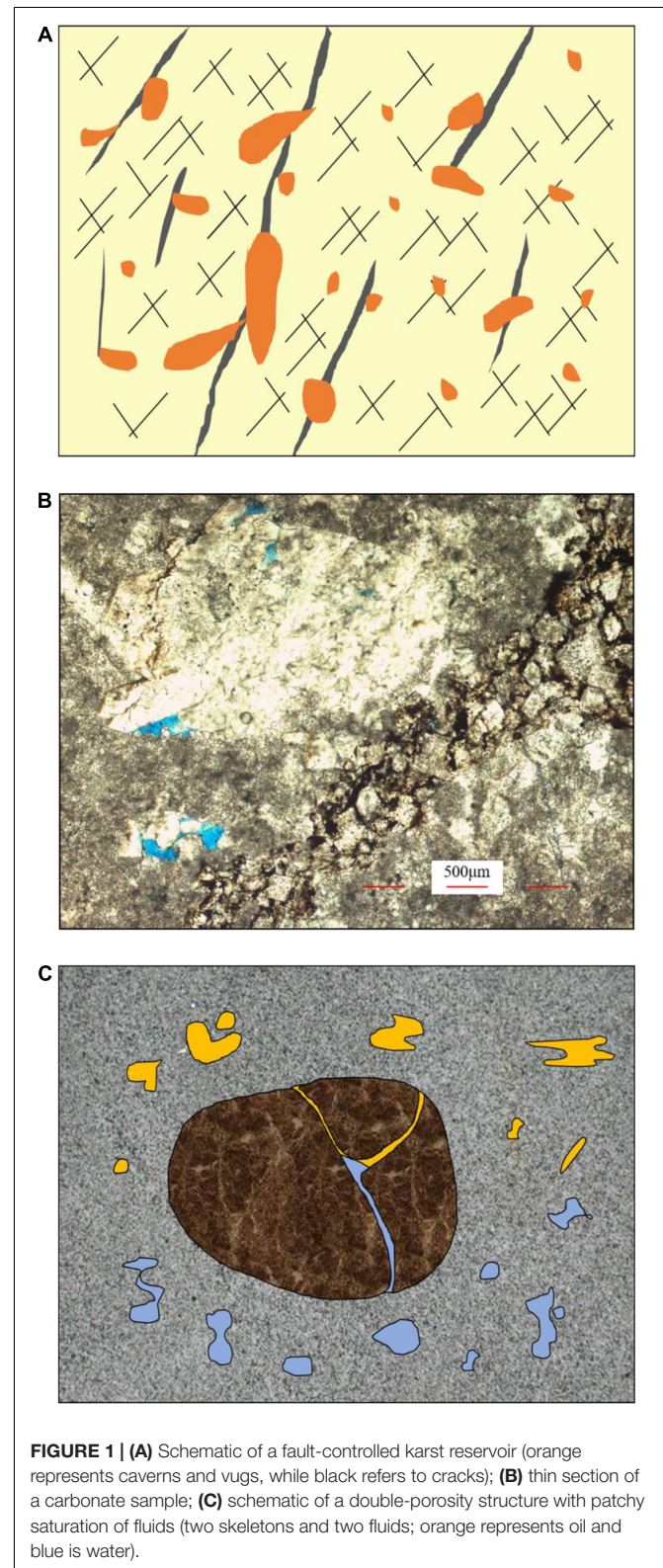
We choose P-wave attenuation, Poisson's ratio and the ratio of the first Lamé constant to mass density ( $\lambda/\rho$ ) to build the templates at ultrasonic and seismic frequencies, based on the DDP theory, and associate the total and crack porosities and oil saturation to the seismic properties. The theory considers the effects of fabric heterogeneity and heterogeneous distribution of immiscible fluids. Ultrasonic, well-log and seismic data are used to calibrate the templates. Then, these are applied to quantitatively predict the rock properties and oil saturation.

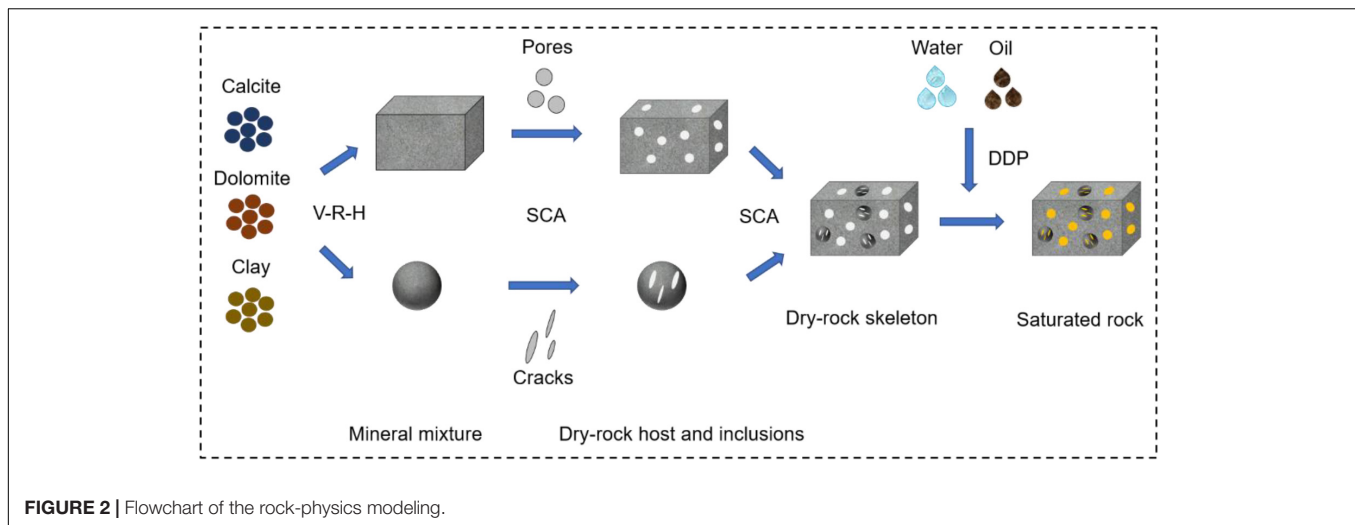
## ROCK-PHYSICS MODEL

### Overview of the Work Area

The area is located at the Tarim Basin, China, and the reservoir section is constituted by the upper members of the Yijianfang to Yingshan formation (Ordovician), formed during the Caledonian-Hercynian period. It is a marine fault-controlled

karst reservoir (Li et al., 2019). The multi-stage fault activity has a controlling effect on the accumulation and distribution of oil and gas in the reservoir. Fractures and fluid transformation





have formed a diverse reservoir system including dissolved pores, inter-crystalline pores and cracks, which make the structure quite complex (Lan et al., 2015). The reservoir along the fault zone is oil-bearing and unevenly enriched. It is characterized by an ultra-deep burial (>7 km), high temperature (>150°C) and high pressure (>160 MPa). **Figure 1A** shows a diagram of the reservoir, where the orange color represents caverns and vugs, and the black lines represent cracks.

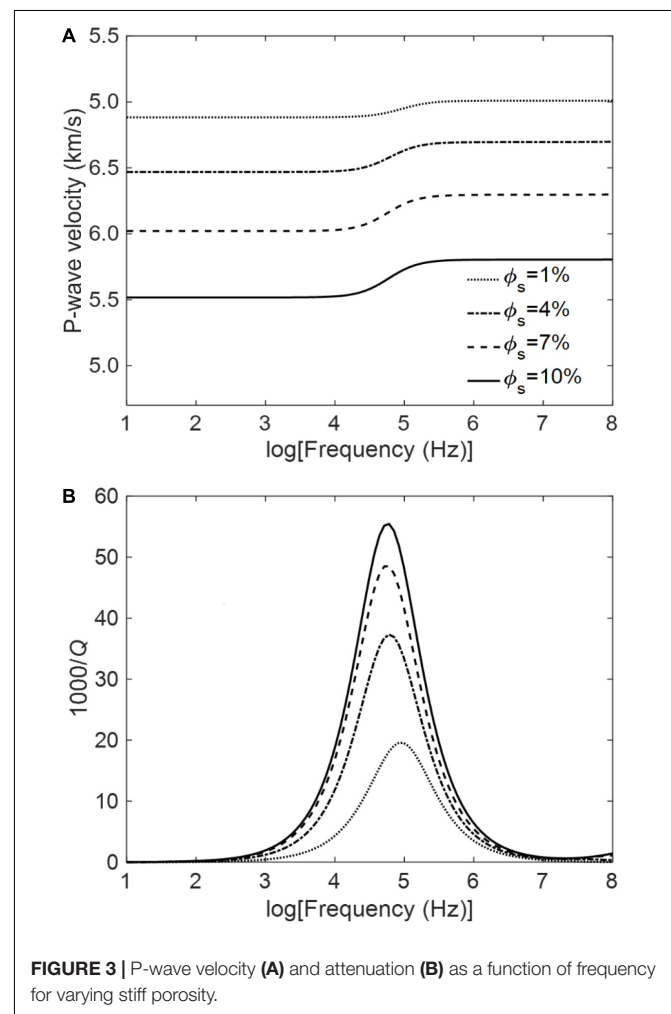
**Figure 1B** shows a thin section of a rock sample collected at a depth of 7443 m. The lithology is limestone, with a dolomite content of 6% and a calcite content of 94%. Dissolution of pores and multiple cracks of various diameters are observed and the surface porosity is extremely low (less than 1%).

## Rock-Physics Modeling Flowchart

The reservoir characteristics are simplified with a double-porosity structure with cracks and pores and saturation with two immiscible fluids, oil and water (**Figure 1C**). **Figure 2** shows the flowchart of the modeling methodology, which can be summarized as follows.

- (1) The minerals are mainly calcite and a small amount of dolomite and clay. The Voigt-Reuss-Hill (VRH) equation (see **Supplementary Appendix Eq. A1**) is used to calculate the elastic moduli of the mineral mixture (Voigt, 1910; Reuss, 1929; Hill, 1952). The bulk and shear moduli of calcite, dolomite, and clay are 63.7 and 31.7, 76.4 and 49.7, and 21 and 7 GPa, respectively (Mavko et al., 2009).
- (2) The pores and cracks are assumed spherical and oblate in shape (Shapiro, 2003), with aspect ratios of 1 and 0.00035 (generally in range of  $10^{-5} \sim 10^{-4}$ , according to Tan et al., 2020 and Pimienta et al., 2015), respectively. The connectivity of these two kinds of pores affects P-wave attenuation and dispersion, as well as the elastic parameters (Agersborg et al., 2008). In this model, the two pore systems are connected and the composite medium is isotropic. Based on the self-consistent approximation (SCA) (Berryman, 1980, 1992, 1998), the pores and cracks

are treated as inclusions and mixed with the minerals to obtain two partial dry-rock elastic moduli and then mixed again with the SCA model to obtain the dry-rock



elastic moduli. At this point, the frame (or skeleton) is a double-porosity structure. The relevant equations are given in **Supplementary Appendix Eq. A2**.

- (3) The volume content of the host medium  $v_1$  and the volume content of inclusion  $v_2$  satisfy  $v_1 + v_2 = 1$ . The total porosity  $\phi = \phi_{10} \cdot v_1 + \phi_{20} \cdot v_2$ , where  $\phi_{10}$  is the porosity of the host medium and  $\phi_{20}$  is the porosity of the inclusions, and the crack porosity is  $\phi_c = \phi_{20} \cdot v_2$ .  $\phi_{20}$  is 0.006 (in range of 0.005~0.1, by considering that a larger cracked grain is modeled as a cylinder of axial length around 100  $\mu\text{m}$ , containing a transverse crack with an average effective aperture of several microns, according to Pride et al., 2004; Pang et al., 2020, and Ba et al., 2017). The stiff porosity is  $\phi_s = \phi - \phi_c$ .

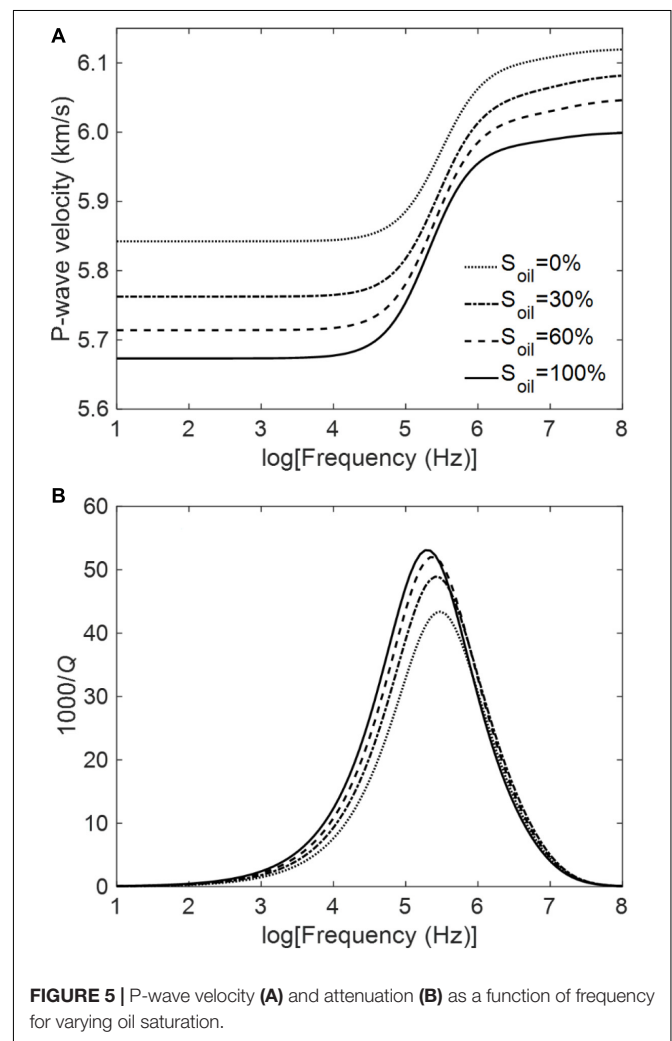
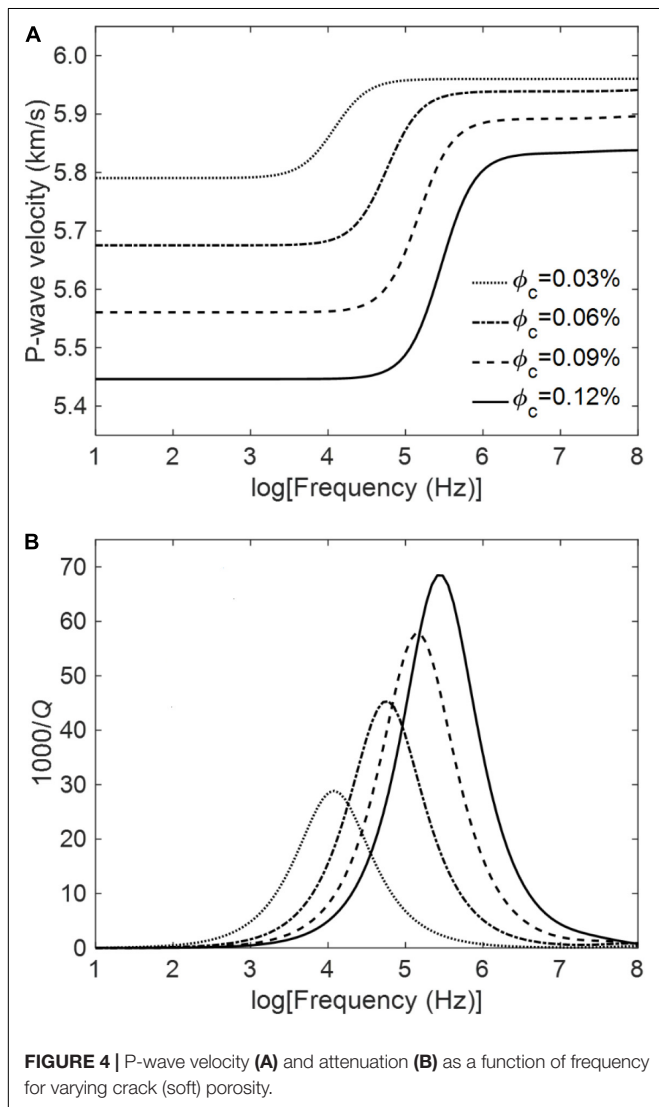
The equations proposed by Batzle and Wang (1992) are used to estimate the bulk moduli, densities, and viscosity of the fluids at 180°C and 80 MPa. The bulk modulus, density, and viscosity of oil and water in the oil-water mixture are 0.79 and 2.2 GPa, 0.70

and 0.93 g/cm<sup>3</sup>, and 0.002289 and 0.000647 Pa s, respectively. Then, fluid substitution is performed by using the DDP theory to obtain the acoustic properties. The main skeleton is composed of two components, namely, a host one with dissolved pores and an inclusion one with cracks, and each of them is patchy saturated. Each component can be considered as a secondary double-porosity structure, i.e., two pore phases saturated with different fluids (there are four types of pores globally). By performing a plane-wave analysis (see **Supplementary Appendix Eq. A5**), we obtain the P-wave velocity and attenuation.

### 3D RPTs

#### P-Wave Phase Velocity and Attenuation

The stiff porosity, crack porosity, and oil saturation are basic factors related to oil production in reservoirs. First, we study the effects of these properties on P-wave velocity and attenuation in the frequency range of  $10^1 \sim 10^8$  Hz. Attenuation is represented by the dissipation factor, defined as  $1000/Q$ , where  $Q$  is the quality factor. Oil saturation is 100%, stiff porosity is 6%, crack porosity

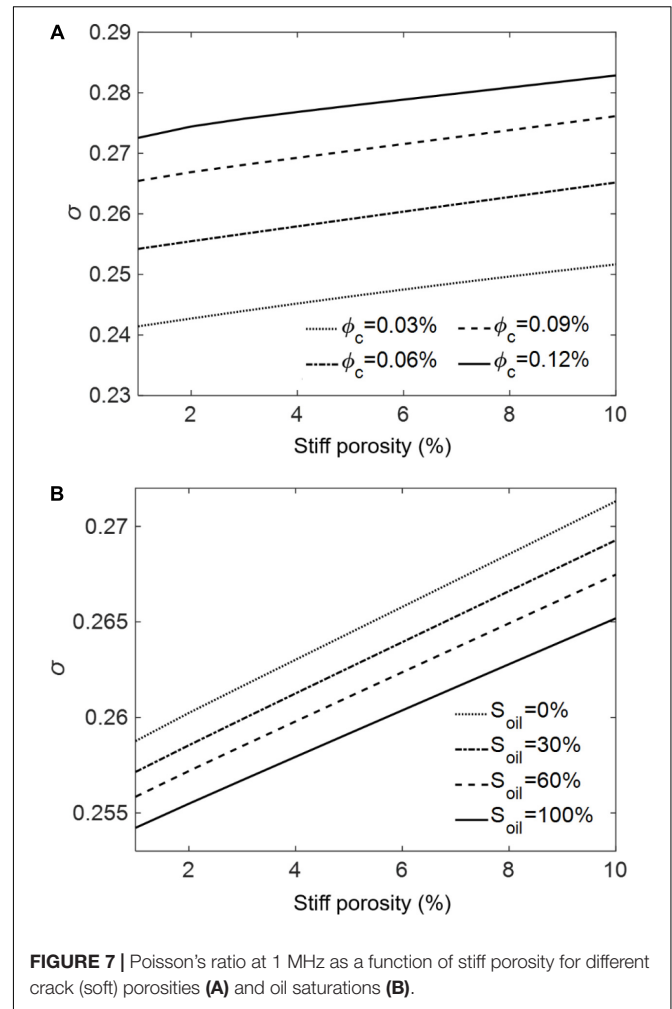
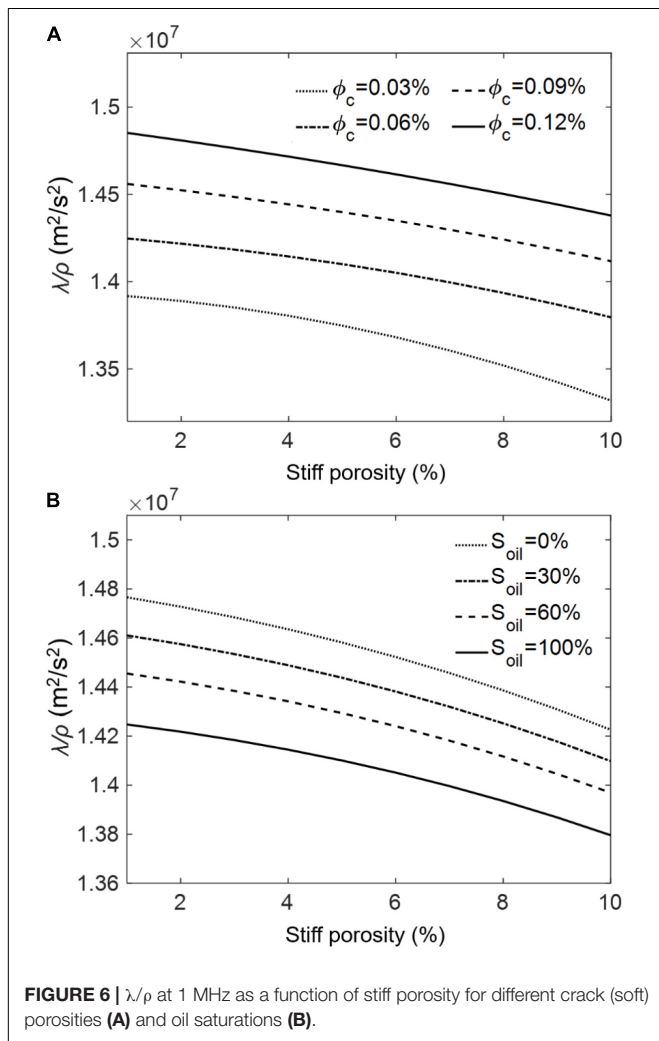


is 0.06%. In the analysis, we vary one property and set the others constant. The fluid patch radius of the host medium is 50  $\mu\text{m}$ , the inclusion radius is 50  $\mu\text{m}$  (at pore/grain scale), and the fluid patch radius in the inclusion is 5  $\mu\text{m}$ .

Figures 3A,B show the effect of the stiff porosity on the P-wave phase velocity and dissipation factor, respectively, where it can be seen that velocity dispersion and attenuation increase with increasing porosity and the relaxation peaks move slightly to the low frequencies. Figure 4 shows that increasing crack porosity, the velocity dispersion becomes stronger, attenuation increases and the peaks move to the high frequencies, while Figure 5 indicates that dispersion and attenuation increase with increasing oil saturation, and the peaks move to the low frequencies.

### Fluid Identification Factors

Poisson's ratio and  $\lambda/\rho$  are used to identify the fluids (Goodway et al., 1997; Quakenbush et al., 2006). Figures 6, 7 show the effects of stiff porosity, crack porosity, and oil saturation at 1 MHz, respectively. As can be seen, increasing stiff porosity and oil saturation,  $\lambda/\rho$  gradually decreases, while increasing crack porosity has the opposite effect. On the other hand (Figure 7),



Poisson's ratio increases with increasing stiff and crack porosities and decreases with increasing saturation.

### Rock-Physics Templates

Total and crack porosities and oil saturation are set as variables to build a 3D RPT at 1 MHz, which is displayed in Figure 8A, where the parameters are the same as in section "P-Wave Phase Velocity and Attenuation." The blue and red line refers to water and oil saturations, respectively, and the behavior of the template agrees with the previous results. On the other hand, Figure 8B shows the 3D RPT at 35 Hz, where the radii of the inclusion, fluid patch in the host medium and fluid patch in the inclusion are 50, 50, and 5 mm, respectively. The characteristics of the seismic template are identical to those of the ultrasonic template.

### CALIBRATION OF THE RPTs

#### Ultrasonic Band

Ultrasonic experiments were performed on five water- and oil-saturated samples at 1 MHz, a pore pressure of 70 MPa and 140°C, whose properties are given in Table 1. The carbonate

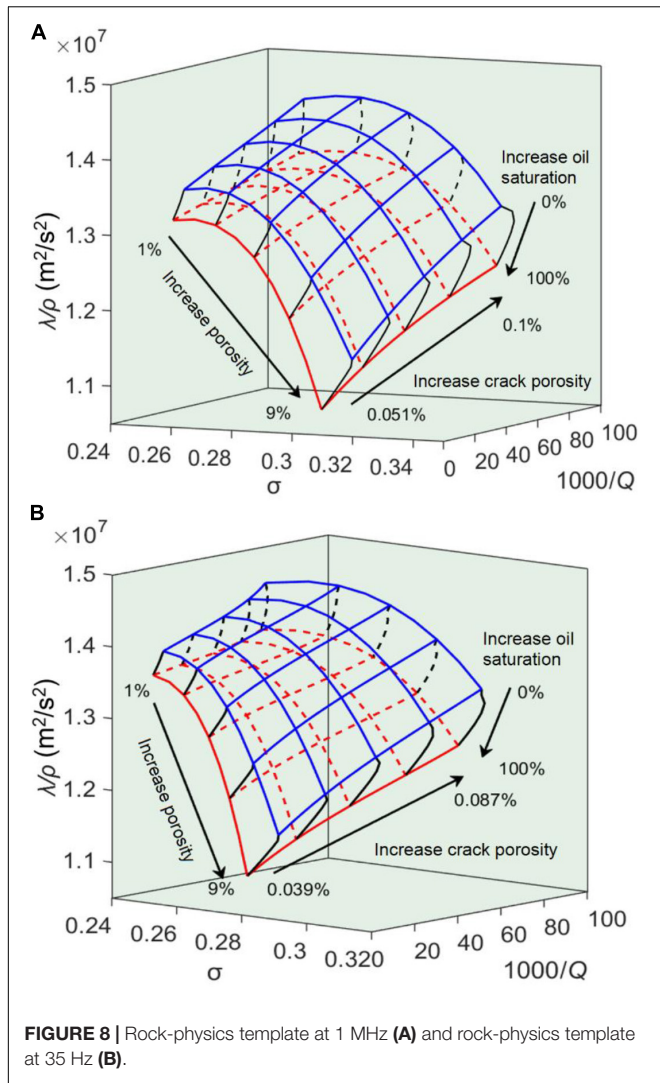
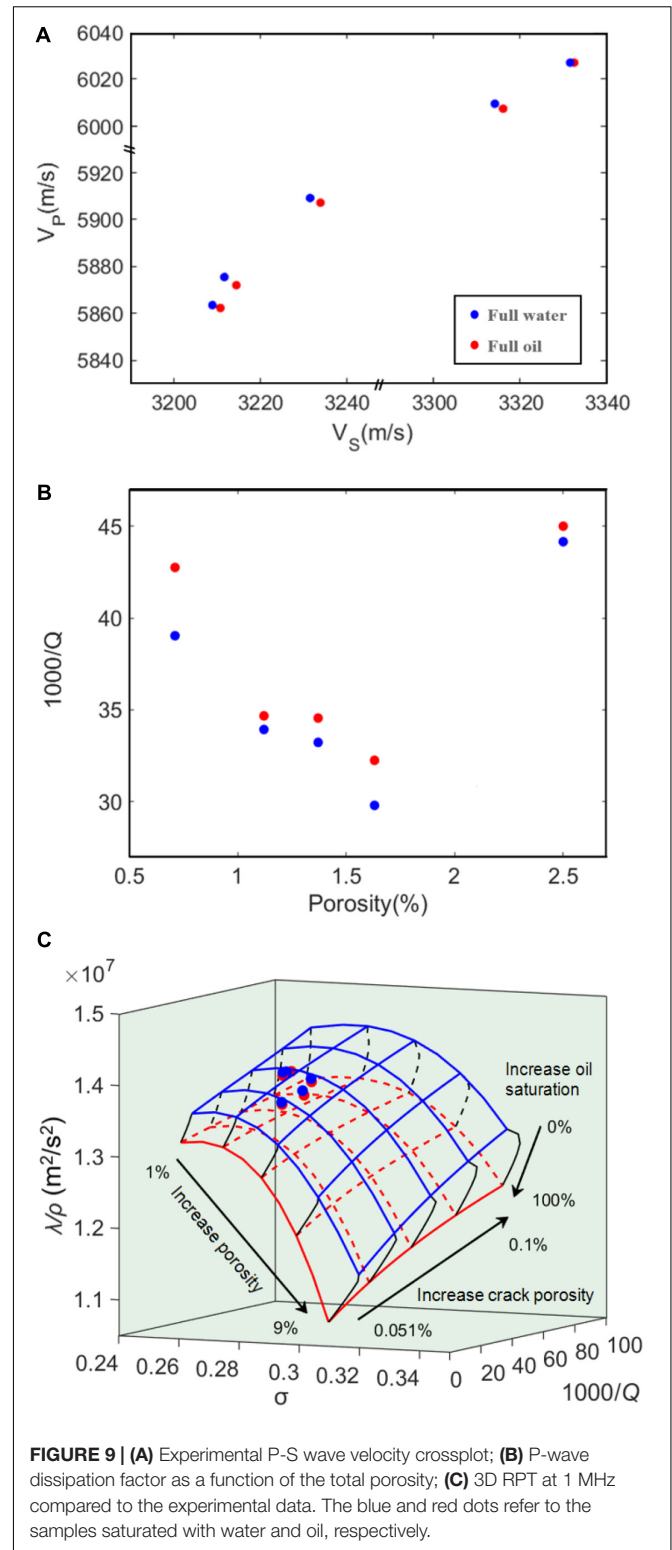


**TABLE 1 |** Properties of the limestone samples.

Sample	A	B	C	D	E
Porosity (%)	1.37	1.12	1.63	0.71	2.50
Dry-rock density (g/cm <sup>3</sup> )	2.67	2.63	2.65	2.67	2.66
Permeability (mD)	0.068	0.051	0.006	1.559	0.023

samples used in the ultrasonic measurements are mainly made of limestone, and parts of cracks are filled with asphalt, calcite, and pyrite. Moreover, there are micro-cracks and a relative amount of dissolved pore cavities. In the experiments, the sample is fully saturated, jacketed, and put into a container according to the experimental setup of Guo et al. (2018a). The first arrivals are picked to obtain the wave velocities. **Figure 9A,B** show the velocities and the attenuation factor estimated with the spectral-ratio method (Toksöz et al., 1979; Guo and Fu, 2006; see **Supplementary Appendix Eq. A3**).

**Figure 9A** shows that P-wave velocity at full water saturation is higher than that at full oil saturation, while the S-wave velocity



exhibits the opposite behavior. **Figure 9B** indicates that the oil-saturated samples have a stronger P-wave attenuation. As shown in the template of **Figure 9C**, the experimental data of these five samples are used for the calibration at ultrasonic frequencies,

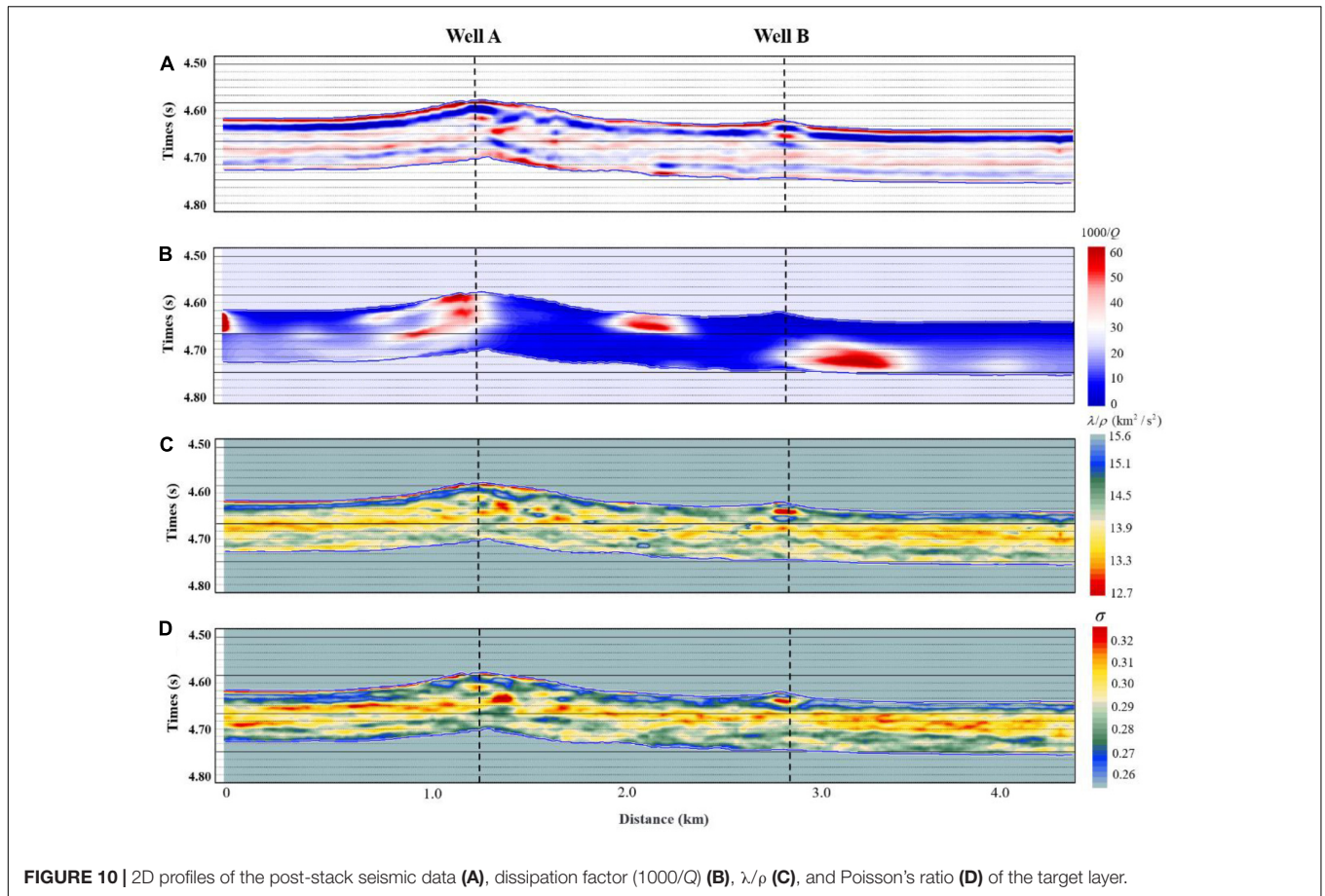


**FIGURE 10** | 2D profiles of the post-stack seismic data (A), dissipation factor ( $1000/Q$ ) (B),  $\lambda/\rho$  (C), and Poisson's ratio (D) of the target layer.

where the blue and red circles refer to the water- and oil-saturated samples, respectively. The average error between the predicted total porosities (based on ultrasonic wave attributes) and the measured porosities under oil saturation is 0.00344. The template shows good agreement with the experimental measurements.

### Seismic Band

Based on well-log and seismic data, the RPT is calibrated at 35 Hz. The seismic quality factor is estimated with the improved frequency-shift method (Pang et al., 2019, 2020), as shown in **Supplementary Appendix Eq. A4**. **Figures 10A,B** show the post-stack seismic data and attenuation (the dissipation factor  $1000/Q$ ) profiles of the target layer, respectively, where the red and blue colors indicate high and low attenuation (**Figure 10B**). The results show that the rocks at the two wells exhibit significant attenuation. On the other hand, Poisson's ratio and  $\lambda/\rho$  are obtained from AVO inversion (Guo et al., 2018b; Luo et al., 2020a,b). The pre-stack angle gather data contains useful information about the amplitude change with angle. The three-parameter inversion method of pre-stack seismic data, based on the AVO theory, can directly estimate P-wave impedance, S-wave impedance and density, and from these the Poisson's ratio and  $\lambda/\rho$  are obtained. **Figures 10C,D** show 2D profiles of  $\lambda/\rho$  and Poisson's ratio obtained with pre-stack seismic inversion. We can see that Poisson's ratio is low in regions with a high  $\lambda/\rho$ .

Attenuation, Poisson's ratio and  $\lambda/\rho$  at well A were used to calibrate the RPT at seismic frequencies (see **Figure 11**) and the log porosity of well A is assumed. Comparing the seismic inversion data with the RPT, we can observe that the seismic data

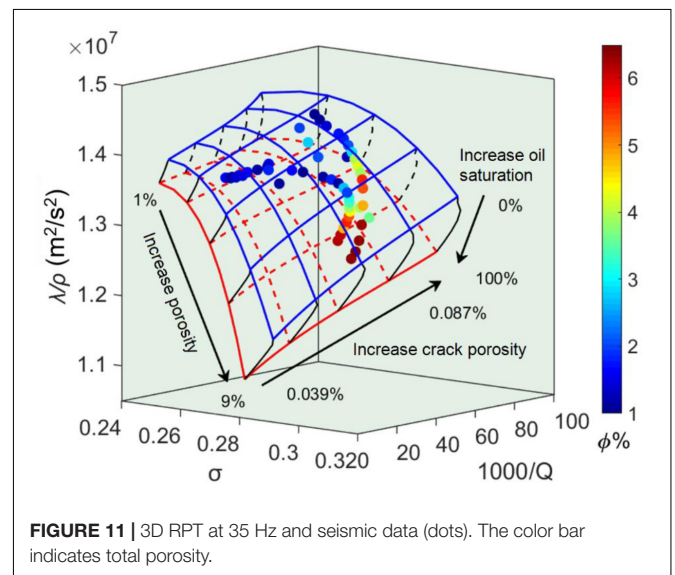


**FIGURE 11** | 3D RPT at 35 Hz and seismic data (dots). The color bar indicates total porosity.

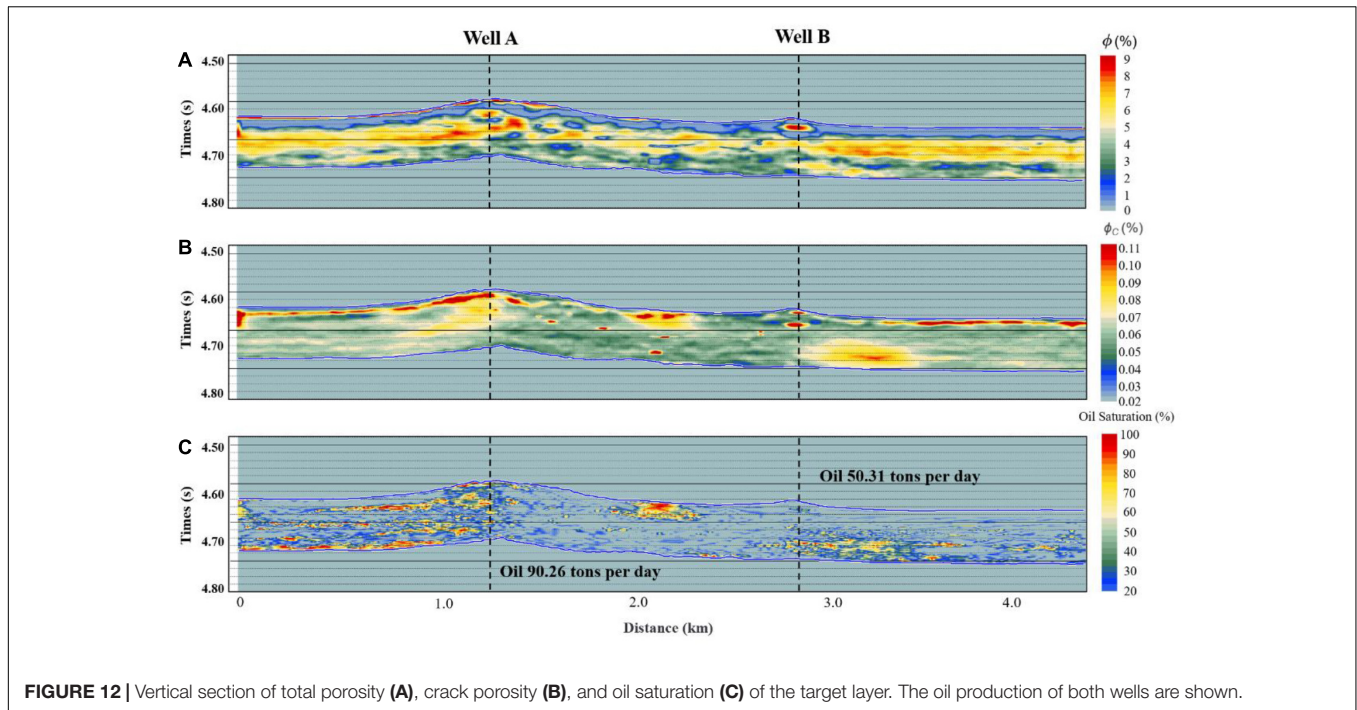


**FIGURE 12** | Vertical section of total porosity (A), crack porosity (B), and oil saturation (C) of the target layer. The oil production of both wells are shown.

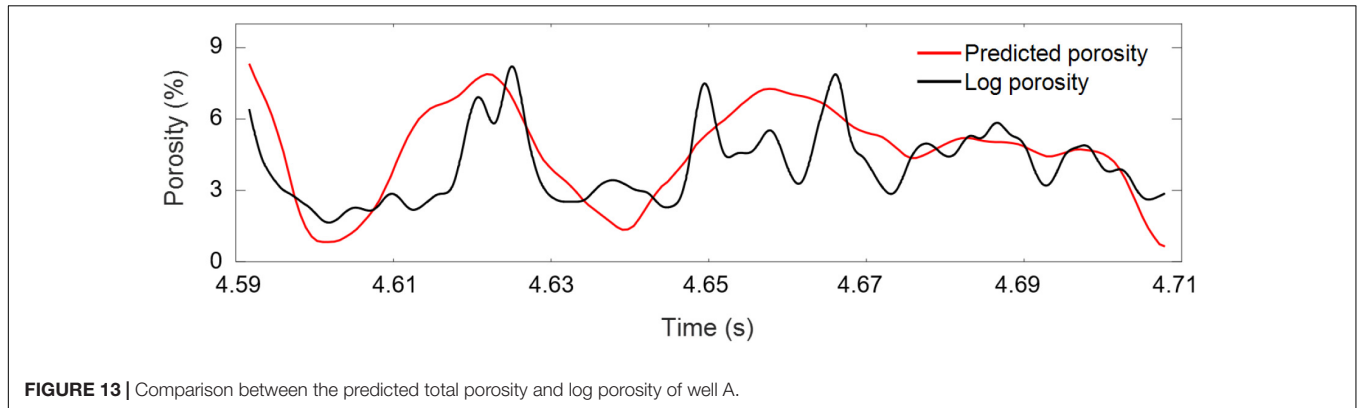


**FIGURE 13** | Comparison between the predicted total porosity and log porosity of well A.

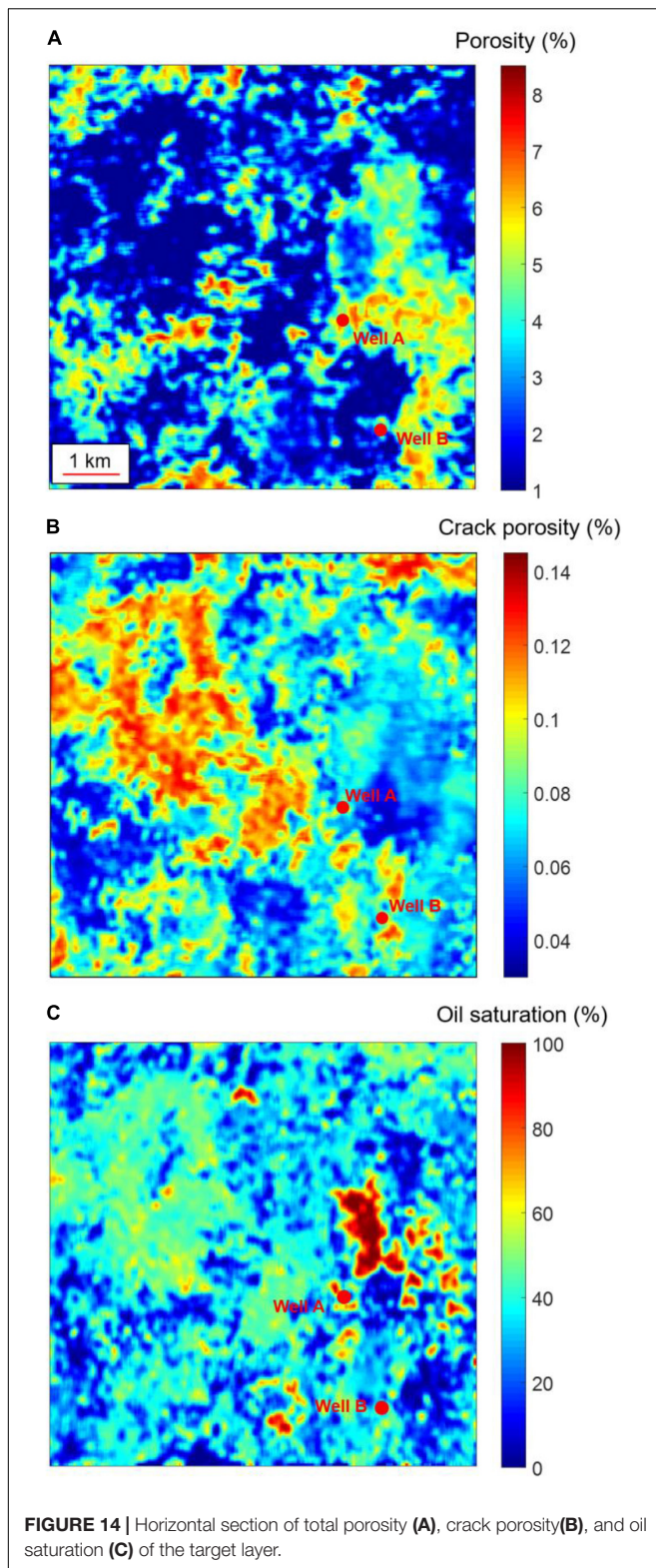
with porosity is consistent with the template. According to the color bar of **Figure 11**, the porosity of the seismic data is low (less than 7%), which agrees with the characteristics of the ultra-deep reservoirs. Attenuation, Poisson's ratio, and  $\lambda/\rho$  can be obtained from seismic data, and a quantitative prediction of total porosity, crack porosity, and oil saturation can be achieved by overlapping the data on the template.

## PREDICTION OF THE RESERVOIR PROPERTIES

The calibrated RPTs are applied to estimate the reservoir properties. **Figure 12** shows the reservoir total and crack porosities, and oil saturation on a 2D survey line crossing wells A and B. In **Figure 12A**, total porosity is generally less than 10% and areas around the wells exhibit higher porosity. As shown in **Figure 13**, the predicted results of well A are consistent with

the porosity log profile. The average error between the predicted porosities (based on seismic wave attributes) and the measured porosities of well A is 0.0125. By combining **Figures 12B,C**, high crack porosity enables good connectivity and better oil storage capacity. In **Figure 12**, we also can see that the upper part of well B has a pore-crack system with low oil saturation, while the lower part has high oil saturation, indicating that the reservoir is not homogeneous. Comparative analysis shows that the predicted results are consistent with the reported oil production of well A (90.26 tons/day) and well B (50.31 tons/day). The prediction results of well A are used to analyze the correlation between crack porosity and oil saturation. The correlation coefficient is 0.6296 between fracture porosity and oil saturation.

**Figure 14** gives horizontal sections of total and crack porosities and oil saturation, showing that well A exhibits higher porosity and oil saturation than well B, while the difference in crack porosity is small. The storage space of fault-controlled karst reservoirs is formed by the dissolution of water or



hydrothermal fluid along the fault and the distribution of the fluid is extremely uneven. Combining **Figures 14A,B**, the distributions of total and crack porosities are complementary and the oil saturation distribution in **Figure 14C** is irregular. These are typical characteristics of fault-controlled karst reservoirs.

It can be seen in **Figures 12, 14** that fault-controlled karst reservoirs do not have a defined oil-water interface, but a patchy fluid saturation due to dissimilar crack-pore characteristics. Crack porosity can be used as an indicator to find regions with high oil saturation. Stiff pores mainly store oil and soft pores act as flow channels and also play an important storage role. These findings are consistent with the actual characteristics of the reservoirs, indicating that the proposed method can be successfully applied.

## CONCLUSION

We have implemented a double double-porosity theory to build RPT in order to estimate the properties of deep carbonate reservoirs. The dry-rock moduli were obtained with a combination of the VRH equation and the self-consistent model. The templates axes involve attenuation, Poisson's ratio and the ratio Lamé constant to density. Ultrasonic experiments were performed on rock samples of the study area and used to calibrate the templates, as well as information from well logs. Then, we have predicted total porosity, crack porosity and oil saturation of the carbonate reservoirs. According to the results, the reservoir has low porosity with developed cracks, which is consistent with the local geological features. Moreover, the results are basically consistent with the actual oil production in the area.

## DATA AVAILABILITY STATEMENT

The original contributions presented in the study are included in the article/**Supplementary Material**, and further inquiries can be directed to the corresponding author/s.

## AUTHOR CONTRIBUTIONS

XZ: ideas and writing. JB: theories and applications. JS and JC: revising. L-YF: suggestions and revising. MP: modeling. All authors contributed to the article and approved the submitted version.

## FUNDING

The authors were grateful to the support of National Natural Science Foundation of China (Grant No. 41821002), the Jiangsu Innovation and Entrepreneurship Plan, Jiangsu Province Science Fund for Distinguished Young Scholars (BK20200021), National Natural Science Foundation of China (41974123), the National Science and Technology Major Project of China (2017ZX05069-002), and the research funds from SINOPEC Key Laboratory of Geophysics.

## SUPPLEMENTARY MATERIAL

The Supplementary Material for this article can be found online at: <https://www.frontiersin.org/articles/10.3389/feart.2021.649984/full#supplementary-material>

## REFERENCES

- Agersborg, R., Johansen, T. A., Jakobsen, M., Sothcott, J., and Best, A. I. (2008). Effects of fluids and dual-pore systems on pressure-dependent velocities and attenuations in carbonates. *Geophysics* 73, N35–N47.
- Ba, J., Carcione, J. M., and Nie, J. X. (2011). Biot-Rayleigh theory of wave propagation in double-porosity media. *J. Geophys. Res. Solid Earth* 116: B06202.
- Ba, J., Xu, W. H., Fu, L. Y., Carcione, J. M., and Zhang, L. (2017). Rock anelasticity due to patchy-saturation and fabric heterogeneity: a double-double porosity model of wave propagation. *J. Geophys. Res. Solid Earth* 122, 1949–1976.
- Batzle, M., and Wang, Z. J. (1992). Seismic properties of pore fluids. *Geophysics* 57, 1396–1408. doi: 10.1190/1.1443207
- Batzle, M., Han, D., and Hofmann, R. (2001). Optimal hydrocarbon indicators. *Paper Presented at the 71st Ann. Internat. Mtg., Soc. Explor. Geophys.*, Tulsa, OK. 1697–1700.
- Berryman, J. G. (1980). Long wavelength propagation in composite elastic media II. ellipsoidal inclusions. *Acoustical Soc. Am. J.* 68, 1820–1831. doi: 10.1121/1.385172
- Berryman, J. G. (1992). Single-scattering approximations for coefficients in Biot's equations of poroelasticity. *Acoustical Soc. Am. J.* 91, 551–571. doi: 10.1121/1.402518
- Berryman, J. G. (1998). Long-wavelength propagation in composite elastic media I. spherical inclusions. *J. Acoustical Soc. Am.* 68, 1809–1819. doi: 10.1121/1.385171
- Carcione, J. M. (2014). *Wave Fields in Real Media, Theory and Numerical Simulation of Wave Propagation in anisotropic, Anelastic, Porous and Electromagnetic Media*, 3rd Edn. Amsterdam: Elsevier.
- Carcione, J. M., and Avseth, P. (2015). Rock-physics templates for clay-rich source rocks. *Geophysics* 80, D481–D500.
- Chi, X. G., and Han, D. H. (2009). Lithology and fluid differentiation using a rock physics template. *Lead. Edge* 28, 60–65. doi: 10.1190/1.3064147
- Deng, J. X., Zhou, H., Wang, H., Zhou, G., and Wang, S. X. (2015). The influence of pore structure in reservoir sandstone on dispersion properties of elastic waves. *Chinese J. Geophys. (in Chinese)* 58, 3389–3400.
- Dillon, L., Schwedersky, G., Guilherme, V., Velloso, R., and Nunes, C. (2003). A multiscale DHI elastic attributes evaluation. *Leading Edge* 22, 1024–1029. doi: 10.1190/1.1623644
- Dvorkin, J., Mavko, G., and Nur, A. (1995). Squirt flow in fully saturated rocks. *Geophysics* 60, 97–107. doi: 10.1190/1.1443767
- Dvorkin, J., Nolen-Hoeksema, R., and Nur, A. (1994). The Squirt-flow mechanism: macroscopic description. *Geophysics* 59, 428–438. doi: 10.1190/1.1443605
- Dvorkin, J., and Nur, A. (1993). Dynamic poroelasticity: a unified model with the squirt and the biot mechanisms. *Geophysics* 58, 524–533. doi: 10.1190/1.1443435
- Goodway, W., Chen, T., and Downton, J. (1997). Improved AVO fluid detection and lithology discrimination using Lamé petrophysical parameters from P and S inversion. *Paper Presented at 67th Annual International Mtg Social. Explor. Geophysics*, Dallas: 183–186.
- Guo, J. X., Shuai, D., Wei, J. X., Ding, P. B., and Gurevich, B. (2018a). P-wave dispersion and attenuation due to scattering by aligned fluid saturated fractures with finite thickness: theory and experiment. *Geophys. J. Int.* 215, 2114–2133. doi: 10.1093/gji/ggy406
- Guo, Q., Zhang, H. B., Han, F. L., and Shang, Z. P. (2018b). Prestack seismic inversion based on anisotropic Markov random field. *IEEE Trans. Geosci. Remote Sens.* 56, 1069–1079. doi: 10.1109/tgrs.2017.2758800
- Guo, M. Q., and Fu, L. Y. (2006). Stress associated coda attenuation from ultrasonic waveform measurements. *Geophys. Res. Lett.* 34:L09307.
- Hedlin, K. (2000). Pore space modulus and extraction using AVO. *Paper presented at 70th Ann. Internat. Mtg., Soc. Explor. Geophys.*, Calgary: 170–173.
- Hill, R. (1952). The elastic behaviour of a crystalline aggregate. *Proc. Phys. Soc.* 65, 349–354. doi: 10.1088/0370-1298/65/5/307
- Johnson, D. L. (2001). Theory of frequency dependent acoustics in patchy-saturated porous media. *J. Acoustical Soc. Am.* 110, 682–694. doi: 10.1121/1.1381021
- Lan, X. D., Lü, X. X., Zhu, Y. M., and Yu, H. F. (2015). The geometry and origin of strike-slip faults cutting the Tazhong low rise megaanticline (central uplift, Tarim Basin, China) and their control on hydrocarbon distribution in carbonate reservoirs. *J. Nat. Gas Sci. Eng.* 22, 633–645. doi: 10.1016/j.jngse.2014.12.030
- Li, Y. Q., Sun, J. F., Wei, H. H., and Song, S. H. (2019). Architectural features of fault-controlled karst reservoirs in the Tahe oilfield. *J. Petroleum Sci. Eng.* 181:106208. doi: 10.1016/j.petrol.2019.106208
- Luo, C., Ba, J., Carcione, J. M., Huang, G. T., and Guo, Q. (2020a). Joint PP and PS pre-stack AVA inversion for VTI medium based on the exact Graebner equation. *J. Petroleum Sci. Eng.* 194:107416. doi: 10.1016/j.petrol.2020.107416
- Luo, C., Ba, J., Carcione, J. M., Huang, G. T., and Guo, Q. (2020b). Joint PP and PS pre-stack seismic inversion for stratified models based on the propagator matrix forward engine. *Surveys Geophys.* 41, 987–1028. doi: 10.1007/s10712-020-09605-5
- Mavko, G., Mukerji, T., and Dvorkin, J. (2009). *The Rock Physics Handbook: Tools for Seismic Analysis of Porous Media*. Cambridge: Cambridge University Press.
- Michel, K. (2010). Rock physics driven inversion: the importance of workflow. *First Break* 28, 68–81.
- Odegaard, E., and Avseth, P. A. (2004). Well log and seismic data analysis using rock physics templates. *First Break* 22, 37–43.
- Pang, M. Q., Ba, J., Carcione, J. M., Picotti, S., Zhou, J., and Jiang, R. (2019). Estimation of porosity and fluid saturation in carbonates from rock-physics templates based on seismic Q. *Geophysics* 84, M25–M36.
- Pang, M. Q., Ba, J., Fu, L. Y., Carcione, J. M., Markus, U. I., and Zhang, L. (2020). Estimation of microfracture porosity in deep carbonate reservoirs based on 3D rock-physics templates. *Interpretation* 8, 1–10. doi: 10.1190/geo2020-0550.1
- Pang, X. Q. (2010). Key challenges and research methods of petroleum exploration in the deep of superimposed basins in western China. *Oil Gas Geol.* 31, 517–534.
- Picotti, S., Carcione, J. M., and Ba, J. (2018). Rock-physics templates for seismic Q. *Geophysics* 84, MR13–MR23.
- Pimienta, L., Fortin, J., and Guéguen, Y. (2015). Bulk modulus dispersion and attenuation in sandstones. *Geophysics* 80, D111–D127.
- Pride, S. R., Berryman, J. G., and Harris, J. M. (2004). Seismic attenuation due to wave induced flow. *J. Geophys. Res.* 109:B01201.
- Qiao, Y. D., and An, H. W. (2007). Study of petrophysical parameter sensitivity from well log data. *Appl. Geophys.* 4, 28–287.
- Quakenbush, M., Shang, B., and Tuttle, C. (2006). Poisson impedance. *Leading Edge* 25, 128–138. doi: 10.1190/1.2172301
- Quintal, B. (2012). Frequency-dependent attenuation as a potential indicator of oil saturation. *J. Appl. Geophys.* 82, 119–128. doi: 10.1016/j.jappgeo.2012.03.001
- Reuss, A. (1929). Calculation of the flow limits of mixed crystals on the basis of the plasticity of monocrystals. *Zeitschrift für Angewandte Mathematik* 9, 49–58.
- Russell, B. H., Gray, D., Hampson, D. P., and Lines, L. (2006). Linearized AVO and poroelasticity. *CREWES Res. Report* 18, 1–25.
- Russell, B. H., Hedlin, K., Hilterman, F. J., and Lines, L. R. (2003). Fluid-property discrimination with AVO: a Biot-Gassmann perspective. *Geophysics* 68, 29–39. doi: 10.1190/1.1543192
- Shapiro, S. A. (2003). Elastic piezosensitivity of porous and fractured rocks. *Geophysics* 68, 482–486. doi: 10.1190/1.1567215
- Tan, W. H., Ba, J., Müller, T., Fang, G., and Zhao, H. B. (2020). Rock physics model of tight oil siltstone for seismic prediction of brittleness. *Geophys. Prospect.* 68, 1554–1574. doi: 10.1111/1365-2478.12938
- Tang, X. M. (2011). A unified theory for elastic wave propagation through porous media containing cracks—An extension of Biot's poroelastic wave theory. *Sci. China Earth Sci.* 54, 1441–1452. doi: 10.1007/s11430-011-4245-7
- Tian, F., Lu, X. B., Zheng, S. Q., Zhang, H. F., Rong, Y. S., Yang, D. B., et al. (2017). Structure and Filling Characters of Paleokarst Reservoirs in Northern Tarim Basin, Revealed by Outcrop, Core and Borehole Images. *Open Geosci.* 9, 266–280.
- Toksöz, M. N., Johnston, D. H., and Timur, A. (1979). Attenuation of seismic waves in dry and saturated rocks: I, Laboratory measurements. *Geophysics* 44, 681–690. doi: 10.1190/1.1440969
- Tran, M., Mukerji, T., and Hosford Scheirer, A. (2020). Lithofacies-dependent rock physics templates of an unconventional shale reservoir on the North Slope, Alaska. *Interpretation* 8, 1–49. doi: 10.1190/int-2019-0156.1
- Voigt, W. (1910). *Lehrbuch der Kristallphysik*. Teubner Leipzig 1928:739.

- White, J. E. (1975). Computed seismic speeds and attenuation in rocks with partial gas saturation. *Geophysics* 40, 224–232. doi: 10.1190/1.1440520
- Xue, J., Gu, H., and Cai, C. (2017). Model-based amplitude versus offset and azimuth inversion for estimating fracture parameters and fluid content. *Geophysics* 82, M1–M17.
- Zou, C. N., Hou, L. H., Hu, S. Y., Zhu, R. K., Liu, S. B., Yang, Z., et al. (2014). Prospect of ultra-deep petroleum onshore China. *Energy Explorat. Exploit.* 32, 19–40. doi: 10.1260/0144-5987.32.1.19

**Conflict of Interest:** The authors declare that the research was conducted in the absence of any commercial or financial relationships that could be construed as a potential conflict of interest.

*Copyright © 2021 Zhou, Ba, Santos, Carcione, Fu and Pang. This is an open-access article distributed under the terms of the Creative Commons Attribution License (CC BY). The use, distribution or reproduction in other forums is permitted, provided the original author(s) and the copyright owner(s) are credited and that the original publication in this journal is cited, in accordance with accepted academic practice. No use, distribution or reproduction is permitted which does not comply with these terms.*